Accepted manuscript of: A. Bekasiewicz, V. Waladi, M. Wojcikowski and T. Dhaene, "Adaptive Wavelet-Based Correction of Non-Anechoic Antenna Measurements," 2023 IEEE Conference on Antenna Measurements and Applications (CAMA), Genoa, Italy, 2023, pp. 795-798, doi: 10.1109/CAMA57522.2023.10352657.

Adaptive Wavelet-Based Correction of Non-Anechoic Antenna Measurements

Adrian Bekasiewicz
Faculty of ETI
Gdansk University of Technology
Gdansk, Poland
bekasiewicz@ru.is

Vorya Waladi
Faculty of ETI
Gdansk University of Technology
Gdansk, Poland
vorya.waladi@pg.edu.pl

Marek Wojcikowski
Faculty of ETI
Gdansk University of Technology
Gdansk, Poland
marek.wojcikowski@pg.edu.pl

Tom Dhaene
Department of Information Technology
Ghent University - imec
Ghent, Belgium
tom.dhaene@ugent.be

***Abstract*—Non-anechoic measurements represent an affordable alternative to evaluation of antenna performance in expensive, dedicated facilities. Due to interferences and noise from external sources of EM radiation, far-field results obtained in non-ideal conditions require additional post-processing. Conventional correction algorithms rely on manual tuning of parameters, which make them unsuitable for reliable testing of prototypes. In this work, a wavelet-based correction method with an adaptively adjusted setup has been proposed. The performance of the presented framework has been demonstrated using an electrically small monopole antenna evaluated in the non-anechoic test site (here, a regular office room). The method has been favorably compared against the existing techniques from the literature.**

Keywords—adaptive correction, antennas, non-anechoic measurements, wavelets, radiation pattern.

I. Introduction

Far-field antenna tests are normally performed in expensive facilities that include anechoic chambers (ACs), compact range, or open-test sites [1]-[6]. Although the mentioned laboratories are capable of ensuring high (specifically, certification-grade) accuracy, their construction costs are prohibitively high [1]-[4]. From this perspective, the use of dedicated facilities might not be justified for certain applications, such as teaching or low-budget research. For the former, the main goal is to demonstrate practical aspects of antenna measurements, and hence their accuracy is not critical. At the same time, the risk of damage to equipment (e.g., due to mishandling by unskilled personnel) is not negligible and might incur high repair costs [1]. From the research perspective, the measurement accuracy is predominantly affected by manual assembly of prototypes, as well as a lack of quality control (e.g., in terms of connectors soldering and/or positioning) [7]-[9]. Furthermore, the connectors are often neglected in the electromagnetic (EM) models of antennas. The consequence is that discrepancies between their simulations and measurements are often inevitable and often considered acceptable [7]-[9].

The antenna radiation performance can also be evaluated in non-anechoic conditions, where strict control over the propagation environment is neglected in favor of installing the measurement gear in locations not designed to support far-field measurements [10]-[13]. Unfortunately, due to the noise from external sources of EM radiation, but also interferences resulting from multi-path propagation between the reference antenna (RA) and the antenna under test (AUT), the performance characteristics obtained in such non-anechoic environments are useless for drawing conclusions on the far-field performance of the radiators [10]-[13].

The problem pertinent to the insufficient accuracy of measurements performed in uncontrolled conditions can be mitigated using appropriate post-processing routines. The available methods fall into two main categories that include: (i) decomposition of noisy responses and (ii) characterization of the propagation environment [10]-[23]. The former class of techniques is oriented towards extracting the relevant part of the RA-AUT response (in time- or frequency-domain) while suppressing unwanted interferences [10]-[20]. Frequency-domain methods involve approximation of the measured responses (based either on the single-, or multi-point analysis) using a composition of carefully selected basis functions such as complex exponentials, spherical coefficients, or Chebyshev polynomials [14]-[17]. Upon identification, the components featuring the highest contribution (e.g., in terms of amplitude) are selected to reconstruct the response whereas the remaining ones are neglected. Temporal approaches, on the other hand, involve conversion of the measured frequency data to the time-domain. The impulse responses are then modified using appropriately selected window functions. The latter ones filter the parts of the signal that do not coincide with Line-of-Sight (LoS) transmission [18]-[20]. The post-processing results are then converted back to the frequency domain to extract the far-field responses. It is worth emphasizing that the discussed algorithms are executed at each angular position of the RA-AUT system. The second class of methods enables extracting the effects of propagation environment on AUT responses based on a series of experiments, or numerical simulations [12], [13], [21]-[23]. In [22], the antenna performance has been determined based on comparative analyses of measurements performed in three different locations within the test site. Another method, proposed in [21], involves EM-simulation-based evaluation of a carefully selected probe antenna in ideal test conditions, as well as in the environment with obstacles. The resulting differential information has been extracted and applied to correct the AUT performance obtained in the non-ideal conditions. A technique oriented towards the characterization of the noise floor of non-anechoic test-site followed by its adaptive filtering from the AUT measurements has been proposed in [12]. The extraction of far-field responses from the equivalent currents calculated on a hull enclosing the radiator under test has also been considered [23].

Regardless of demonstrated usefulness, the existing post-processing methods are difficult to setup and prone to failure [10]-[12], [15]-[23]. Their performance-related parameters are normally tuned in a manual, or semi-manual fashion (i.e., through physical analysis of the test-site dimensions, or based on visual inspection of the impulse response) [10], [11], [18]. Consequently, the state-of-the-art algorithms are of limited use for less-experienced engineers. Another problem is that the techniques are predominantly validated in idealized conditions, i.e., ACs with installed reflective surfaces, or EM simulation environments [15]-[18], [21], [24]. The former are substantially less challenging (propagation-wise) compared to, e.g., hallways or office rooms, where the interferences and

the external noise cannot be attenuated [10], [11], [13]. At the same time, the simulation-based setups are stationary in time (due to a lack of noise from external sources and/or other time-variant distortions), which also simplifies analysis [21]. Another problem is that the correction procedures are predominantly validated using electrically large, high-gain radiators [6], [10], [11]. Due to improved signal-to-noise ratio, extraction of their characteristics is much less of a challenge compared to compact (e.g., planar) radiators [7], [13]. From this perspective, the problem concerning the reliable refinement of antenna far-field measurements performed in non-anechoic conditions remains unsolved.

In this work, a framework for adaptive, wavelet-based correction of far-field performance characteristics obtained in uncontrolled environments has been proposed. The method involves the automatic identification of the LoS-delay profile within the RA-AUT system, which is then used to facilitate the wavelet-based post-processing of the signal. The presented approach has been demonstrated using a geometrically small ultra-wideband monopole antenna evaluated in the non-anechoic test site (here, office room) at four frequencies of interest. The technique has been favorably compared against the state-of-the-art techniques from the literature.

II. Methodology

Let $\boldsymbol{R}(\boldsymbol{\omega}, \boldsymbol{\theta})$ be the family of S_{21} responses measured in the non-anechoic test site. Here, $\boldsymbol{\omega} = [\omega_1 \ \ldots \ \omega_K]^T$ is the sweep around the center frequency of interest $f_0 = (\omega_K - \omega_1)/2$ and $\boldsymbol{\theta} = [\theta_1 \ \ldots \ \theta_A]^T$ denotes the angle of AUT rotation ($a = 1, \ldots, A$) w.r.t. the reference antenna. The goal of the correction process is to perform the transformation h: $\boldsymbol{R} \rightarrow \boldsymbol{R}_c$, where $\boldsymbol{R} = \boldsymbol{R}(\boldsymbol{\omega}, \boldsymbol{\theta})$; $\boldsymbol{R}_c = \boldsymbol{R}_c(f_0, \boldsymbol{\theta})$ is the far-field response at f_0 as a function of $\boldsymbol{\theta}$ refined using a set of wavelet-based kernel functions [25]. The post-processing procedure h consists of the following two steps.

The first step involves identification of the LoS delay between the RA-AUT system components as a function of θ_a angle. Let $\boldsymbol{P}(\boldsymbol{t}, \theta_a) = \boldsymbol{T}(\boldsymbol{t}, \theta_a) \circ \boldsymbol{T}(\boldsymbol{t}, \theta_a)^*$ be the time-domain-based power characteristic, where $\boldsymbol{T}(\boldsymbol{t}, \theta_a) = F^{-1}(\boldsymbol{R}(\boldsymbol{\omega}, \theta_a), N)$ is the N-point impulse response. Here, $N = 2^{\lceil \log_2(K) \rceil + 3}$ (with $\lceil \cdot \rceil$ being the round up to the nearest integer) [13]. The symbols $F^{-1}(\cdot)$, "$\circ$", "*" denote an inverse Fourier transform, component-wise multiplication, and conjugate transpose, respectively [26]. The time-domain sweep is given as $\boldsymbol{t} = [t_1, \ldots, t_N]^T = \partial t \cdot \boldsymbol{M}$ with the step of $\partial t = B^{-1} = (\omega_K - \omega_1)^{-1}$, and $\boldsymbol{M} = [-N/2, \ldots, N/2-2, N/2-1]^T$. The LoS profile is extracted based on a bi-stage, automatic analysis of $\boldsymbol{P} = \boldsymbol{P}(\boldsymbol{t}, \theta_a)$ responses. In the initial phase ($j = 1$), the individual components of the LoS vector (as a function of θ_a) $\boldsymbol{d}^{(j)} = [d_1^{(j)} \ \ldots \ d_A^{(j)}]^T$ are calculated from:

$$d_a^{(j)} = \underset{\substack{d_a^{(j)} \in \boldsymbol{t} \\ d_l^{(j)} \le d_a^{(j)} \le d_h^{(j)}}}{\arg\max} \left(\boldsymbol{P}\left(\boldsymbol{t}, \theta_a\right) \right) \tag{1}$$

In equation (1), the lower- and upper-bounds for seeking the power pulse maxima are $d_l^{(1)} = 0$ and $d_h^{(1)} = \partial t \cdot (N/2-1)$, respectively. It should be noted, however, that the challenging propagation conditions—resulting from multi-path interferences, as well as a lack of noise-suppressing mechanisms—might result in erroneous identification of the $\boldsymbol{d}^{(j)}$ vector components. This has been demonstrated and discussed in [13]. Here, the problem is mitigated through resetting of the algorithm (1), i.e., with $j = 2$, within the refined bounds $d_l^{(2)} = d_{\text{opt}} - \beta \cdot h_0$ and $d_h^{(2)} = d_{\text{opt}} + \beta \cdot h_0$, where $d_{\text{opt}} = \min(\boldsymbol{t}_d^{(1)})$ represents the shortest LoS distance (and hence the delay) between the RA and AUT. The parameters h_0 and β denote the half-prominence of the LoS power pulse (i.e., its width at the middle of height) and time-based scaling (here, set to $\beta = 3$) [25]. The motivation behind restricting LoS identification around d_{opt} is that the expected change in the RA-AUT delay is small. Hence, any delayed signal featuring higher amplitude than for a peak identified in the vicinity of d_{opt}, would be a result of multi-path propagation (e.g., as reflection from the metallic components located in the test-site) [13]. The final LoS profile, obtained as a result of bi-stage analysis, i.e., $\boldsymbol{d}^* = \boldsymbol{d}^{(2)} = [d_1^{(2)} \ \ldots \ d_a^{(2)} \ \ldots \ d_A^{(2)}]^T$ is used for adaptive centering of the individual wavelet-based kernel functions.

The second step of the correction process is oriented towards modification of the non-anechoic responses using Morlet wavelets. Figure 1 shows a comparison of the example RA-AUT transmission and a Gaussian function (both normalized) [25]. It should be noted that their shapes are similar (especially in the time-instances that correspond to the LoS signal). The response also demonstrates that the analysis of $\boldsymbol{P}$ might be less of a challenge compared to the impulse response. This is because the latter one features more complex transitions around LoS transmission. The wavelet kernel used in this work is of the form:

$$\boldsymbol{T}_\kappa(\boldsymbol{t}, \theta_a) = \exp\left(2\left(j\pi f_0 \left(\boldsymbol{t} - d_a^*\right) - \frac{1}{4}\left(\pi f_0 \left(\boldsymbol{t} - d_a^*\right)\right)^2 \right) \right) \tag{2}$$

where $d_a^* = d_a^{(2)}$ denote the components of the LoS profile. The consequence of adjusting (2) w.r.t. $\boldsymbol{d}^*$ elements is that the resulting kernels are centered around the fraction of $\boldsymbol{T}(\boldsymbol{t}, \theta_a)$ response corresponding to the LoS-delays extracted from $\boldsymbol{P}(\boldsymbol{t}, \theta_a)$.

The corrected performance characteristic of the antenna at hand (w.r.t. a set of θ_a angles) is obtained as:

$$\boldsymbol{T}_c\left(\boldsymbol{t}, \theta_a\right) = \boldsymbol{T}_\kappa(\boldsymbol{t}, \theta_a) \circ \ \boldsymbol{T}(\boldsymbol{t}, \theta_a) \tag{3}$$

Next, $\boldsymbol{T}_c(\boldsymbol{t}, \theta_a)$ is converted to the frequency domain using the Fourier transform as $\boldsymbol{R}_c(\boldsymbol{\Omega}, \theta_a) = F(\boldsymbol{T}_c(\boldsymbol{t}, \theta_a), N)$ [26]. Note that $\boldsymbol{\Omega} = \partial\omega \cdot \boldsymbol{M} - (\omega_K - \omega_1)/2$ and $\partial\omega = 1/(t_N - t_1)$. The above procedure is repeated for all $\boldsymbol{\theta}$ angles. Finally, the corrected response is extracted at the frequency of interest ($f_0 \in \boldsymbol{\Omega}$) as:

$$\boldsymbol{R}_c\left(f_0, \boldsymbol{\theta}\right) = \left[R_c\left(f_0, \theta_1\right) \ldots R_c\left(f_0, \theta_A\right) \right]^T \tag{4}$$

The presented correction algorithm can be summarized as follows:

1. Obtain $\boldsymbol{R}(\boldsymbol{\omega}, \boldsymbol{\theta})$ in non-anechoic environment;
2. Analyze $\boldsymbol{P}(\boldsymbol{t}, \theta_a)$ to extract $\boldsymbol{d}^*$ and adjust wavelet-based kernel parameters;
3. Obtain $\boldsymbol{R}_c(\boldsymbol{\Omega}, \boldsymbol{\theta})$ from the corrected time-domain data (3) and extract $\boldsymbol{R}_c(f_0, \boldsymbol{\theta})$ using (4).

Note that analysis of $\boldsymbol{P}(\boldsymbol{t}, \theta_a)$ and automatic identification of $\boldsymbol{d}^*$ are crucial for adjusting the wavelet kernel location (time-wise) and hence maintaining high correction accuracy. It is worth noting that the presented framework does not rely on engineering insight (especially in terms of identifying the

relevant intervals of the RA-AUT responses). From this perspective, the method represents a notable improvement (setup-wise) compared to the state-of-the-art algorithms from the literature [10]-[12], [15]-[18].

III. Results

Performance of the proposed correction scheme has been demonstrated using the electrically small spline-parameterized monopole antenna of Fig. 2 [13]. The structure has been validated in the non-anechoic test site of Fig. 3. Apart from the installation of the positioning towers and active equipment, the room is not tailored to far-field measurements. Its dimensions are 5.5 × 4.5 × 3.1 m^3. The experiments have been performed at the following set of frequencies f_0 = {3.1, 4.5, 5.8, and 8.5} GHz. The bandwidth and the number of points required to perform signal analysis have been set—based on recommendations from [13]—to B = 3 GHz and K = 201, respectively. All of the obtained characteristics have been compared against the anechoic chamber measurements.

The non-anechoic data have been refined using the methodology of Section II. A family of the yz-direction radiation patterns (cf. Fig. 2) extracted before and after correction is shown in Fig. 4. The obtained results indicate that a very high distortion of the uncorrected characteristics (resulting from multi-path propagation and the external noise) renders them useless for drawing conclusions on a real-world antenna performance. At the same time, the refined responses highly resemble the radiation patterns obtained in the anechoic chamber. The correction performance—expressed in terms of the root-mean-square error (RMSE)—averaged over the number of considered frequencies amounts to –30.8 dB which represents a 16.6 dB improvement w.r.t. uncorrected characteristics. From this perspective, the quality of the responses obtained as a result of post-processing using the proposed method is excellent. The numerical results are summarized in Table I.

The performance of the method has also been validated (using the same dataset) against state-of-the-art routines from the literature. For a fair comparison, the setup of all algorithms in terms of K and B remains unchanged. The considered benchmark techniques are based on time-gating with (i) rectangular and (ii) Hann functions [26]. The post-processing parameters (i.e., window intervals) have been determined as a result of: (i) analysis of the test site dimensions and (ii) visual inspection of the RA-AUT impulse response (in the time-domain) [10], [11], [18]. The results gathered in Table I indicate that the proposed approach outperforms the competitive algorithms by a large margin in terms of the correction performance. For the considered antenna and frequencies, the average RMSE for the responses corrected using (i) and (ii) amounts to –15 dB and –20 dB, which correspond to only 0.9 dB and 5.9 dB improvement w.r.t. direct measurements in the given test site (compared to over 16 dB gain when using the presented algorithm). It should be emphasized that the proposed method was also capable of maintaining almost 13.6 dB improvement of the response fidelity compared to AC at the 5.8 GHz frequency (up to almost 4 dB better w.r.t. benchmark algorithms), which is a part of the spectrum shared with existing communication system (i.e., WiFi).

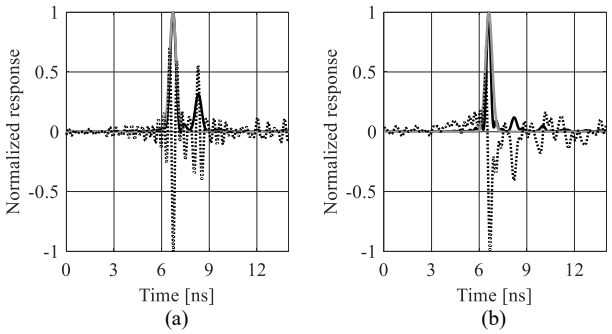

Fig. 1. Comparison of the time-domain-based RA-AUT responses before correction (black) for impulse $\boldsymbol{T}(t, \theta_a)$ (···) and power $\boldsymbol{P}(t, \theta_a)$ (—) against Gaussian pulse (gray) at: (a) 3.1 GHz and (b) 5.8 GHz frequencies. Note that, due to high variability in time, reliable analysis of $\boldsymbol{T}(t, \theta_a)$ is difficult.

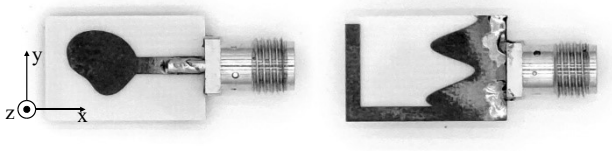

Fig. 2. A photograph of the electrically small spline-parameterized monopole antenna considered for experiments [13].

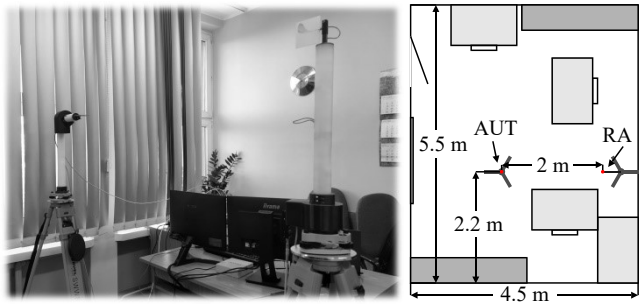

Fig. 3. A photograph (left) and schematic view of the on-anechoic test site considered for experiments.

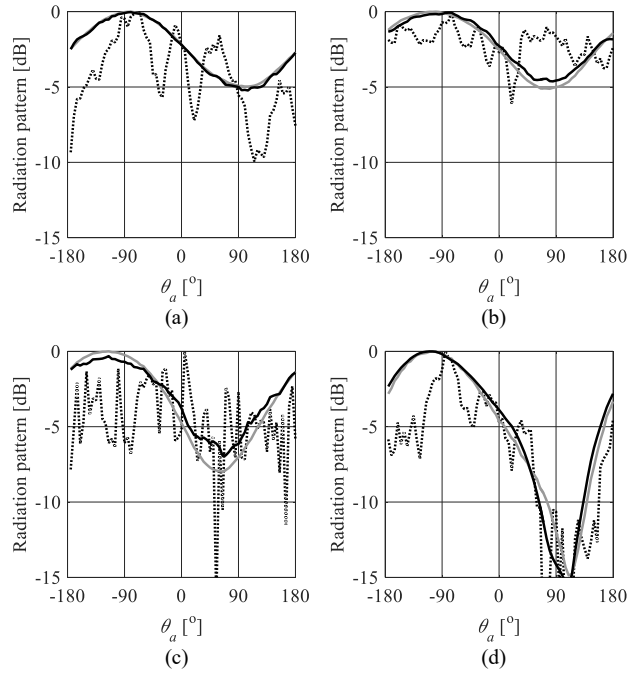

Fig. 4. Compact monopole antenna: non-anechoic responses (black) before (···) and after (—) refinement vs. AC measurements (gray) at: (a) 3.1 GHz, (b) 4.5 GHz, (c) 5.8 GHz, and (d) 8.5 GHz frequencies.

TABLE I. BENCHMARK OF THE PROPOSED METHOD

Method	Uncorrected	(i)	(ii)	This work
3.1 GHz (RMSE)	–14.11 dB	–8.19 dB	–15.01 dB	–37.63 dB
4.5 GHz (RMSE)	–16.31 dB	–15.25 dB	–20.30 dB	–31.51 dB
5.8 GHz (RMSE)	–11.78 dB	–15.54 dB	–21.45 dB	–25.36 dB
8.5 GHz (RMSE)	–14.34 dB	–20.91 dB	–23.50 dB	–28.50 dB
Average RMSE	–14.14 dB	–14.97 dB	–20.07 dB	–30.75 dB

IV. CONCLUSION

In this work, a wavelet-based framework for post-processing of far-field measurements performed in non-anechoic environments has been proposed. The method involves identification of the LoS profile based on analysis of power responses (extracted as functions of angular positions between the RA and AUT), followed by adjustment of wavelet kernels w.r.t. the extracted delays. The performance of the presented algorithm has been demonstrated based on measurements of the electrically small, spline-parameterized monopole antenna in the test-site (office room) that has not been tailored to far-field experiments. The obtained results indicate that, for the considered radiator and the test conditions, the average performance improvement—due to the use of the proposed algorithm—amounts to over 16 dB RMSE. The method has also been favorably compared against the state-of-the-art algorithms from the literature. The benchmark results indicate performance improvement resulting from the use of the presented framework is up to 10 dB higher as compared to the existing post-processing methods.

Future work will focus on enhancing the presented correction scheme to enable automatic identification of the bandwidth around the frequency of interest, as well as the number of frequency-domain points required for accurate post-processing. The combination of the proposed method with other algorithms in order to maximize the amount of information that can be extracted from one-shot measurements will also be considered.

ACKNOWLEDGMENT

This work was supported in part by the National Science Center of Poland Grant 2021/43/B/ST7/01856, National Center for Research and Development Grant NOR/ POLNOR/HAPADS/0049/2019-00, as well as Gdansk University of Technology (Excellence Initiative – Research University) Grant 16/2023/IDUB/IV.2/EUROPIUM.

REFERENCES

[1] L. Hemming, *Electromagnetic Anechoic Chambers: A fundamental Design and Specification Guide*, IEEE Press, Piscataway, 2002.

[2] E.F. Knott, *et al*., *Radar Cross Section*, 2nd ed., Artech House, Boston, 1993.

[3] W.D. Burnside, *et al.*, "An enhanced tapered chamber design," *Ant. Meas. Tech. Assoc. Proc.*, Monterey Bay, CA, 1999.

[4] X. Li, L. Chen, Z. Wang, K. Yang, and J. Miao, "An ultra-wideband plane wave generator for 5G base station antenna measurement," *Electronics*, vol. 12, art no. 1824, 2022.

[5] F. Zhang, Y. Zhang, Z. Wang, and W. Fan, "Plane wave generator in non-anechoic radio environment," *IEEE Ant. Wireless Prop. Lett*., 2023.

[6] S. Kurokawa, M. Hirose, and K. Komiyama, "Measurement and uncertainty analysis of free-space antenna factors of a log-periodic antenna using time-domain techniques," *IEEE Trans. Instrumentation Meas.*, vol. 58, no. 4, pp. 1120-1125, April 2009.

[7] M.S. Khan, *et al.*, "A compact CSRR-enabled UWB diversity antenna," *IEEE Ant. Wireless Prop. Lett.*, vol. 16, pp. 808-812, 2017.

[8] A. Bekasiewicz and S. Koziel, "Structure and design optimisation of compact UWB slot antenna," *Electronics Lett.*, vol. 52, no. 9, pp. 681-682, 2016.

[9] S. Koziel, A. Bekasiewicz, and Q.S. Cheng, "Conceptual design and automated optimization of a novel compact UWB MIMO slot antenna," *IET Microwaves, Ant. Prop.*, vol. 11, no. 8, pp. 1162-1168, 2017.

[10] A. Soltane, G. Andrieu, E. Perrin, C. Decroze, and A. Reineix, "Antenna radiation pattern measurement in a reverberating enclosure using the time-gating technique," *IEEE Ant. Wireless Prop. Lett.*, vol. 19, no. 1, pp. 183-187, 2020.

[11] P. Piasecki and J. Strycharz, "Measurement of an omnidirectional antenna pattern in an anechoic chamber and an office room with and without time domain signal processing," *Signal Proc. Symp.*, pp. 1-4, Debe, Poland, 2015.

[12] A.N. de Sao Jose, V. Deniau, U.C. Resende, and R. Adriano, "Improving antenna gain estimations in non-ideal test sites with auto-tunable filters," *Measurement*, vol. 159, art no. 107720, 2020.

[13] A. Bekasiewicz, S. Koziel, and M. Czyz, "Time-gating method with automatic calibration for accurate measurements of electrically small antenna radiation patterns in non-anechoic environments," *Measurement*, vol. 208, art no. 112477, 2023.

[14] Y. Su and S. Gong, "Reflection suppression through modal filtering for wideband antenna measurement in a non-absorbent environment," *Electronics*, vol. 11, no. 20, art. no. 3422, 2022.

[15] Z. Du, J.I. Moon, S.-S. Oh, J. Koh, and T.K. Sarkar, "Generation of free space radiation patterns from non-anechoic measurements using Chebyshev polynomials," *IEEE Trans. Ant. Prop.*, vol. 58, no. 8, pp. 2785-2790, 2010.

[16] B. Fourestie, Z. Altman, J. Wiart, and A. Azoulay, "On the use of the matrix-pencil method to correlate measurements at different test sites," *IEEE Trans. Ant. Prop.*, vol, 47, no. 10, pp. 1569-1573, 1999.

[17] G. Leon, S. Loredo, S. Zapatero, and F. Las-Heras, "Radiation pattern retrieval in non-anechoic chambers using the matrix pencil algorithm," *Prog. EM. Res. Lett*., vol. 9, pp. 119-127, 2009.

[18] S. Loredo, M.R. Pino, F. Las-Heras, and T.K. Sarkar, "Echo identification and cancellation techniques for antenna measurement in non-anechoic test sites," *IEEE Ant. Prop. Mag.*, vol. 46, no. 1, pp. 100-107, 2004.

[19] R.V. de Jong, M. Hajian, and L.P. Ligthart, "Antenna time-domain measurement techniques," *IEEE Ant. Prop. Mag.*, vol. 39, no. 5, pp. 7-12, 1997.

[20] F.G. Awan, and A. Kiran, "Cancellation of interference for emission measurement in open area test site," *Measurement*, vol. 111, pp. 183-196, 2017.

[21] J. Koh, A. De, T.K. Sarkar, H. Moon, W. Zhao, and M. Salazar-Palma, "Free space radiation pattern reconstruction from non-anechoic measurements using an impulse response of the environment," *IEEE Trans. Ant. Prop.*, vol. 60, no. 2, pp. 821-831, 2012.

[22] S.M. Froes, P. Corral, M.S. Novo, M. Aljaro, and A.C.C. Lima, "Antenna radiation pattern measurement in a nonanechoic chamber," *IEEE Ant. Wireless Prop. Lett.*, vol. 18, no. 2, pp. 383-386, 2019.

[23] J. Knapp, J. Kornprobst, and T.F. Eibert, "Equivalent source and pattern reconstruction from oversampled measurements in highlyreflective environments," *IET Microwaves, Ant. Prop.*, vol. 13 no. 13, pp. 2232-2241, 2019.

[24] P. Gonzalez-Blanco and M. Sierra-Castaner, "Analysis of time filtering techniques for echo reduction in antenna measurements," *Int. J. Microwave Wireless Tech.*, vol, 9, no. 7, pp. 1387-1395, 2017.

[25] M.X. Cohen, *Analyzing Neural Time Series Data: Theory and Practice*, MIT Press, 2014.

[26] A.V. Oppenheim, R.W. Schafer, *Discrete-Time Signal Processing*, 3rd ed., Prentice Hall, 2009.